targets

MDPI

Article

Photo-Cleavable Polycations-Wrapped Upconversion Nanoparticles for Efficient siRNA Delivery and Cancer Therapy

Yuling He [1,2,*], Shuwen Guo [3], Huangxian Ju [1] and Ying Liu [1,*]

[1] Shaanxi Key Laboratory of Brain Disorders, Institute of Basic and Translational Medicine, Xi'an Medical University, No. 1 Xinwang Road, Xi'an 710021, China; hxju@nju.edu.cn
[2] State Key Laboratory of Analytical Chemistry for Life Science, School of Chemistry and Chemical Engineering, Nanjing University, Nanjing 210023, China
[3] Key Laboratory of Analytical Chemistry for Life Science of Shaanxi Province, School of Chemistry and Chemical Engineering, Shaanxi Normal University, Xi'an 710100, China; guoshuwen@snnu.edu.cn
* Correspondence: heyuling0925@163.com (Y.H.); yingliu@nju.edu.cn (Y.L.)

Abstract: RNA interference (RNAi) therapy is a promising approach for cancer therapy. However, due to the weak binding affinity between a carrier and small interference RNA (siRNA) and complicated tumor environment, efficient loading and release of siRNA still remain challenging. Here, we design photo-cleavable polycations-wrapped upconversion nanoparticles (PC-UCNPs) for spatially and temporally controllable siRNA delivery. The PC-UCNPs are synthesized by in situ reversible addition−fragmentation chain transfer (RAFT) polymerization of photo-cleaved 5-(2-(dimethylamino)ethoxy)-2-nitrobenzyl acrylat (MENA) monomer and poly(oligo(ethylene oxide) methyl ether acrylate (OEMA) mononer through a chain transfer agent that anchored on the surface of silica-coated upconversion nanoparticles (UCNPs@SiO_2). After reacting with CH_3I, siRNA and hyaluronic acid (HA) are adsorbed on the particle surface to prepare PC-UCNPs/siRNA/HA. The reaction with cell-secreted hyaluronidase (HAase) achieves the intracellular delivery of PC-UCNPs/siRNA/HA, and 980 nm laser irradiation causes siRNA release, which effectively improves the gene silencing efficiency in vitro and suppresses tumor growth in vivo; therefore, these processes have a promising potential application in precision medicine.

Keywords: polycations; Upconversion Nanoparticles (UCNPs); photo-cleavage; siRNA delivery

Citation: He, Y.; Guo, S.; Ju, H.; Liu, Y. Photo-Cleavable Polycations-Wrapped Upconversion Nanoparticles for Efficient siRNA Delivery and Cancer Therapy. *Targets* **2023**, *1*, 63–78. https://doi.org/10.3390/targets1010006

Academic Editor: David Ulmert

Received: 28 June 2023
Revised: 6 September 2023
Accepted: 7 September 2023
Published: 12 September 2023

1. Introduction

Gene interference therapy using exogenous small interfering RNA (siRNA) to selectively silence gene expression and inhibit protein transcription has become a promising cancer therapeutic approach [1–3]. However, the key challenge for the further application of RNA interference (RNAi) therapy still remains in the efficient delivery and release of these small, fragile biomolecules. Currently, many types of responsive siRNA delivery systems have been developed with pH [4,5], small molecule [6], light irradiation [7,8] and temperature [9] as stimuli, which enhances the controllability for gene release and the efficiency of gene transfection.

Light irradiation is a promising strategy for the on-demand release of payload [10–12]. Recently, near-infrared (NIR) light has attracted much attention due to its minimal photodamage on living tissues, low auto-fluorescence background, non-photobleaching and deep penetration [13–15]. The lanthanide-doped upconversion nanoparticles (UCNPs) can absorb long-wavelength NIR light and generate short-wavelength UV and visible light emissions [16,17]. The integration of UCNPs with photoresponsive molecules, including o-nitrobenzy [18], spiropyran [19] and azobenzene [20], have been studied for drug delivery, gene delivery and in vitro/in vivo imaging [18,21]. Although NIR-regulated UCNPs delivery systems have been reported for the successful release of siRNA [22,23], surface-loaded siRNA usually lacks protection, impairing loading efficiency and resulting in siRNA

degradation or leakage during the delivery process [24,25]. Therefore, a NIR-responsive siRNA delivery system with a satisfactory loading capacity, stability and release efficiency is needed with urgency.

With the positive charge and convenience for functionalization, cationic polymers could enhance siRNA loading efficiency [26–29]. Here, we designed NIR-cleavable polycations-encapsulated UCNPs for efficient siRNA delivery and tumor therapy. UCNPs are coated with SiO_2 and functionalized with chain transfer reaction (CTA) initiator 2-(((propanethio) carbonothioyl)thio)acetic acid. Reversible addition−fragmentation chain transfer (RAFT) polymerization is then carried out on the UCNPs surface with photo-responsive 5-(2-(dimethylamino)ethoxy)-2-nitrobenzyl acrylate (MENA) and poly(oligo(ethylene oxide) methyl ether acrylate (OEMA) as monomers. After reacting with CH_3I, the as-obtained PC-UCNPs subsequently absorb siRNA and hyaluronic acid (HA) via electrostatic interactions to obtain PC-UCNPs/siRNA/HA (Scheme 1a). The outer layer of negatively charged HA not only extends blood circulation but also achieves siRNA delivery specificity by recognizing the CD44 receptor on the tumor cell membrane. The degradation of HA by hyaluronidase (HAase) exposes inner cationic polymers and promotes intracellular delivery and lysosome escape. Upon subsequent 980 nm laser irradiation, the UV emission of UCNPs cleaves the photosensitive o-nitrobenzyl segment and detaches the polymer coating from the UCNPs surface for efficient siRNA release (Scheme 1b). This strategy demonstrates the effective silencing of target gene expression and suppression of tumor growth; therefore, it should become a universal strategy for efficient NIR-assisted gene therapy.

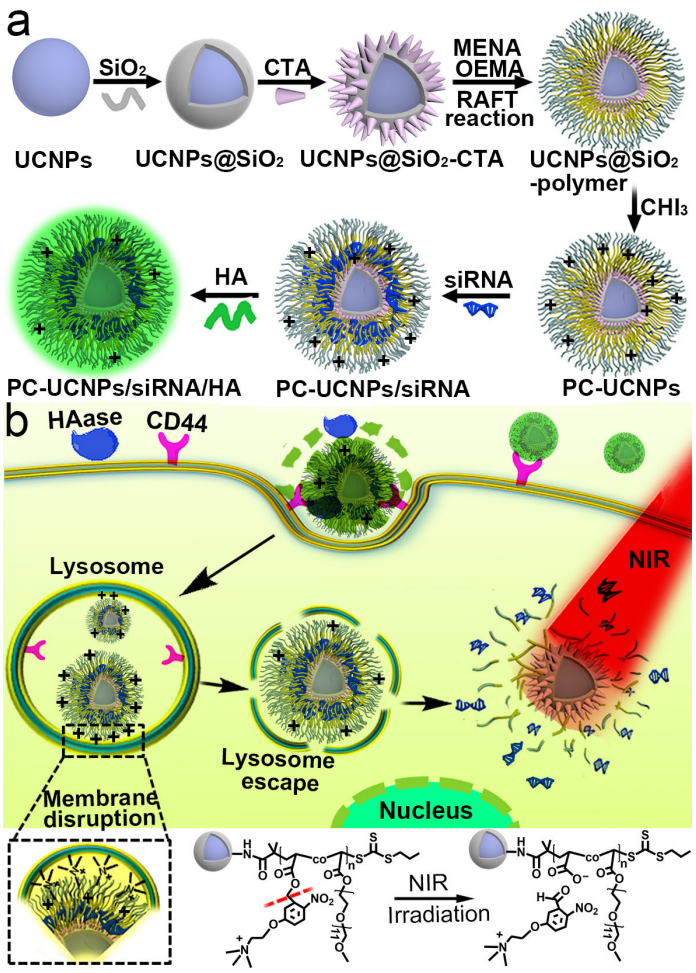

Scheme 1. Schematic illustration of (**a**) synthesis and (**b**) intracellular delivery of PC-UCNPs/siRNA/HA with NIR responsive siRNA release.

2. Results and Discussion

2.1. Synthesis and Characterization of UCNPs@SiO_2-Polymer

UCNPs core $NaYF_4$:Yb,Tm was synthesized using the previously reported solvent thermal method [30] and coated with an $NaYF_4$ shell to prevent the influence of surface defects and enhance particle luminescence [31]. The as-obtained core–shell-structured UCNPs $NaYF_4$:Yb,Tm@$NaYF_4$ was further coated with a thin silica layer using a reverse-phase microemulsion method to obtain UCNPs@SiO_2 [32]. The synthesized UCNPs with an average size of 29 ± 2.82 nm is shown in Figure 1a.

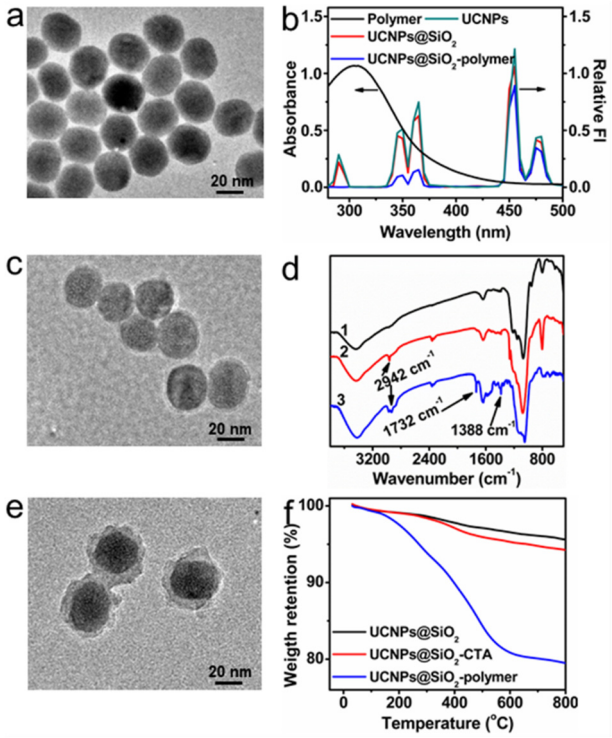

Figure 1. TEM image of (**a**) UCNPs, (**c**) UCNPs@SiO_2, and (**e**) UCNPs@SiO_2-polymer, (**b**) Upconversion luminescence spectra of UCNPs (green line), UCNPs@SiO_2 (red line), PC-UCNPs (blue line) and UV–Vis absorption spectrum of polymer (black line), (**d**) FT-IR spectra of (1) UCNPs@SiO_2, (2) UCNPs@SiO_2-CTA and (3) UCNPs@SiO_2-polymer, (**f**) Thermogravimetric analysis of UCNPs@SiO_2, UCNPs@SiO_2-CTA and UCNPs@SiO_2-polymer.

Emission peaks at 290 nm, 345 nm and 363 nm correspond to $^1I_6 \rightarrow {}^3H_6$, $^1I_6 \rightarrow {}^3F_4$ and $^1D_2 \rightarrow {}^3H_6$ transitions of Tm^{3+}, respectively, and 455 nm and 475 nm correspond to $^1D_2 \rightarrow {}^3F_4$ and $^1G_4 \rightarrow {}^3H_6$ transitions of Tm^{3+}, respectively (Figure 1b, green line). SiO_2 coating increased the size of UCNPs@SiO_2 to 31 ± 2.1 nm (Figure 1c), which had little effect on UCNPs emissions (Figure 1b, red line). The chain transfer agent, 2-(((propanethio) carbonothioyl)thio)acetic acid (CTA) (Figure S1, Supplementary Materials), was conjugated to UCNP@SiO_2 via the amide bond. The as-obtained UCNPs@SiO_2-CTA demonstrated a CTA characteristic absorption peak at 305 nm in the UV-Vis spectrum (Figure S2) and –CH_2– characteristic absorption peak at 2942 cm^{-1} corresponding to C–H stretching vibration in the FT-IR spectrum (Figure 1d, UCNPs@SiO_2-CTA). Reversible addition−fragmentation chain transfer (RAFT) polymerization of 5-(2-(dimethylamino)ethoxy)-2-nitrobenzyl acrylate (MENA) (Figures S3–S5) and Poly(oligo(ethylene glycol)) methyl ether acrylate (OEMA) was conducted on the surface of UCNP@SiO_2-CTA as the RAFT agent (Figure S6), which obtained P(OEMA-co-MENA)-conjugated UCNPs (UCNPs@SiO_2-polymer) with a size of 44 ± 1.7 nm and a thickness corresponding to a polymer shell, 6 ± 0.9 nm (Figure 1e). The molecular mass of as-obtained P(OEMA-co-MENA) on UCNPs surface was measured via Gel permeation chromatographic (GPC) analysis as 11.6 kDa (Figure S7). The character-

istic absorbance of UCNPs@SiO_2-polymer in the range of 280–440 nm overlapped with the emission of UCNPs@SiO_2 at 290 nm, 345 nm and 375 nm (Figure 1b, black line, red line), which led to a substantial decrease in UCNPs emission peak at 290 nm, 345 nm and 375 nm (Figure 1b, blue line). Moreover, the FT-IR spectrum of UCNPs@SiO_2-polymer showed the new absorbance peak at 1732 cm^{-1} corresponding to stretching vibrations of the ester group and at 1388 cm^{-1} corresponding to stretching vibrations of -NO_2 compared with UCNPs@SiO_2-CTA (Figure 1d, UCNPs@SiO_2-polymer). In addition, thermogravimetric analysis of UCNPs@SiO_2-polymer showed about 19% of weight loss (Figure 1f, UCNPs@SiO_2-polymer). These results demonstrated that RAFT polymerization was successfully initiated on the surface of UCNPs@SiO_2-CTA.

2.2. Preparation of PC-UCNPs/siRNA/HA and In Vitro Verification of HA Degradation and siRNA Release

To load negatively charged siRNA via electrostatic interaction, the tertiary amine groups from UCNPs@SiO_2-polymer were reacted with CH_3I to form quaternary ammonium salts. Compared with UCNPs@SiO_2-polymer, the as-obtained PC-UCNPs had an increased zeta potential of 58 ± 2.2 mV, while its hydrodynamic diameter remained unchanged (Figure S8). A series amount of siRNA was loaded on PC-UCNPs, and the weight ratio of PC-UCNPs/siRNA was optimized as 1/1, as indicated by the significantly retarded siRNA band in agarose gel retardation assay (Figure 2a). HA was further coated with PC-UCNPs/siRNA to obtain PC-UCNPs/siRNA/HA. After siRNA loading, the as-obtained PC-UCNPs/siRNA showed a zeta potential of 26 ± 2.3 mV and a hydrodynamic diameter of 61 ± 1.9 nm (Figure 2b, PC-UCNPs/siRNA). Continuous surface modification of HA decreased zeta potential to −23 ± 2.6 mV due to carboxylate groups of HA and increased the hydrodynamic diameter of particles to 70 ± 2.5 nm (Figure 2b, PC-UCNPs/siRNA/HA).

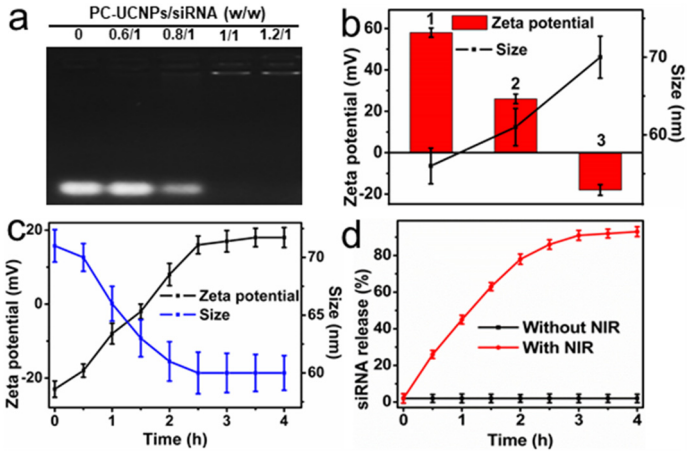

Figure 2. (**a**) Agarose gel retardation assay for PC-UCNPs/siRNA at various weight ratios (*w*/*w*). (**b**) Zeta potential and DLS analysis of (1) PC-UCNPs, (2) PC-UCNPs/siRNA, (3) PC-UCNPs/siRNA/HA. (**c**) Zeta potential and DLS analysis of PC-UCNPs/siRNA/HA in response to HAase at different time points. (**d**) The release curve of siRNA from PC-UCNPs/siRNA/HA as a function of time in response to NIR irradiation. The error bars indicate means ± SD (*n* = 4).

The serum stability of the delivery carrier is important to prolong circulation time and elevate tumor targeting [33]. The hydrodynamic diameter and polydispersity index (PDI) of PC-UCNPs/siRNA/HA remained unchanged when incubated with DMEM containing 10% fetal bovine serum (Figure S9), indicating the satisfactory stability of PC-UCNPs/siRNA/HA.

The negatively charged surface of PC-UCNPs/siRNA/HA can effectively extend systemic circulation time [34] and respond to internal tumor microenvironments for surface charge conversion to facilitate intracellular delivery. Due to the surface-adsorbed HA, PC-UCNPs/siRNA/HA was recognized by the CD44 membrane receptor. The HA coat-

ing layer was then degraded by the overexpressed HAase enzyme in the tumor cell [35], which exposed the positively charged surface of PC-UCNPs/siRNA to achieve the intracellular delivery and endosomal escape of PC-UCNPs/siRNA/HA. According to the HA degradation period, the zeta potential of PC-UCNPs/siRNA/HA continued its increase towards 25 ± 2.4 mV, indicating the gradual decomposition of negatively charged HAs and exposure of the positively charged PC-UCNPs/siRNA surface (Figure 2c, zeta potential). Along with the degradation of HA, the hydrodynamic size of PC-UCNPs/siRNA/HA continued its decrease to 62 ± 2.7 nm (Figure 2c, size), which was similar to that of PC-UCNPs/siRNA (Figure 2b, PC-UCNPs/siRNA, size), indicating the complete degradation of HA from the UCNPs surface. SiRNA release was achieved via external NIR irradiation, and siRNA-loaded PC-UCNPs/siRNA/HA with NIR irradiation showed rapid release, and the release percentage saturated at around 92% at 3 h (Figure 2d). On the contrary, PC-UCNPs/siRNA/HA showed a negligible release of siRNA (2%) in the absence of NIR irradiation (Figure 2d), indicating a satisfactory precise control of siRNA release via NIR light irradiation.

2.3. Internalization of PC-UCNPs/siRNA/HA and Intracellular siRNA Release

After the degradation of the HA coating layer, the highly cationic surface of PC-UCNPs/siRNA could facilitate the lysosomal escape of PC-UCNPs/siRNA. Acridine orange (AO) assay was conducted to monitor the lysosomal membrane permeabilization of HepG2 cells. HepG2 cells were incubated with PBS, UCNPs@SiO_2-polymer, PC-UCNPs/HA, and PC-UCNPs/siRNA/HA, respectively, and stained with AO. Strong green fluorescence was observed from PBS-treated HepG2 cells and UCNPs@SiO_2-polymer-treated HepG2 cells (Figure 3a, PBS, UCNPs@SiO_2-polymer), while declined green fluorescence and increased red fluorescence was observed from PC-UCNPs/HA and PC-UCNPs/siRNA/HA-treated HepG2 cells (Figure 3a, PC-UCNPs/HA, PC-UCNPs/siRNA/HA), proving the contribution of cationic surface to lysosomal membrane permeabilization. A lysosomal colocalization experiment was further performed to trace the internalization and lysosomal escape of PC-UCNPs/siRNA/HA by CLSM images. FAM labelled siRNA (siRNA-FAM) was used to prepare PC-UCNPs/siRNA-FAM/HA, which demonstrated good overlap of green fluorescence of FAM and red fluorescence of Lysotracker Red after 2 h incubation, confirming efficient internalization of PC-UCNPs/siRNA-FAM/HA (Figure 3b, 2 h). After 6 h of incubation, the FAM fluorescence had spread to the entire cytoplasm, while the lysosome probe showed weaker fluorescence due to the acidity dependence of Lysotracker red (Figure 3b, 6 h) [36], indicating the efficient lysosomal escape of PC-UCNPs/siRNA-FAM/HA.

To verify the successful release of siRNA from PC-UCNPs to cytoplasm, PC-UCNPs/siRNA-FAM/HA was incubated with HepG2 cells for 4 h, and UCNPs emission at 454 nm and 475 nm and FAM emission at 529 nm was monitored via CLSM. Separation of FAM fluorescence (green channel) and UCNPs fluorescence (red channel) was observed for PC-UCNPs/siRNA-FAM/HA-treated HepG2 cells after 40 min of NIR light irradiation (Figure 4a, NIR(+)), indicating the efficient release of siRNA from PC-UCNPs. On the contrary, no fluorescence separation was observed for PC-UCNPs/siRNA-FAM/HA-treated HepG2 cells in the absence of NIR irradiation (Figure 4a, NIR(−)).

HA-mediated endocytosis specificity was further confirmed by CLSM images. Strong intracellular FAM fluorescence was observed for PC-UCNPs/siRNA-FAM/HA incubated HepG2 cells (Figure 4b, HepG2), while excess HA pretreated HepG2 cells showed little fluorescence after incubation with PC-UCNPs/siRNA/HA (Figure 4b, HA pretreated HepG2). Moreover, the semiquantitative analysis of intracellular FAM-siRNA fluorescence also showed higher intensity for HepG2 cells than HepG2 cells pretreated with HA (Figure S10). These results indicated good targeting specificity for HA-mediated cancer cell internalization.

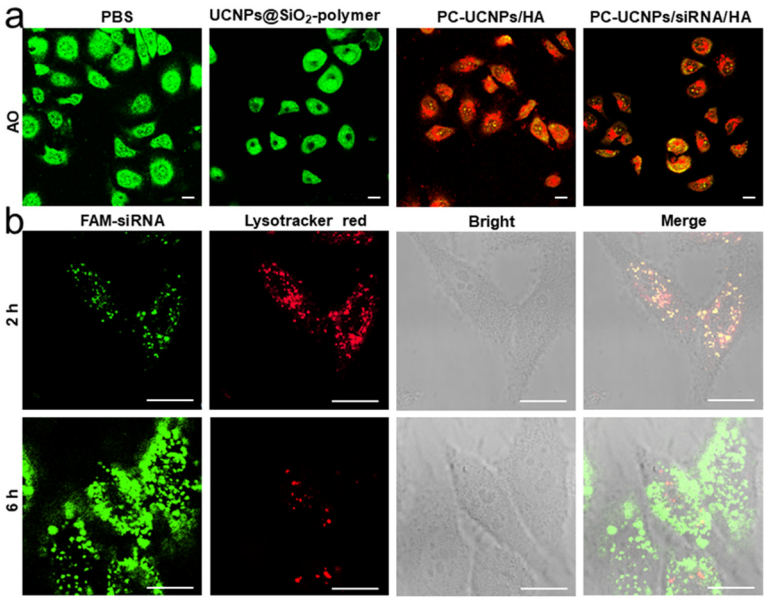

Figure 3. Confocal microscopic images of (**a**) AO-stained HepG2 cells treated with PBS, UCNPs@SiO_2-polymer, PC-UCNPs/HA and PC-UCNPs/siRNA/HA (with 10 nM siRNA loading, Scale bar: 20 μm), (**b**) colocalization of lysosome and PC-UCNPs/siRNA/HA when incubated with HepG2 cells for different durations (With 10 nM siRNA loading, Scale bar: 8 μm).

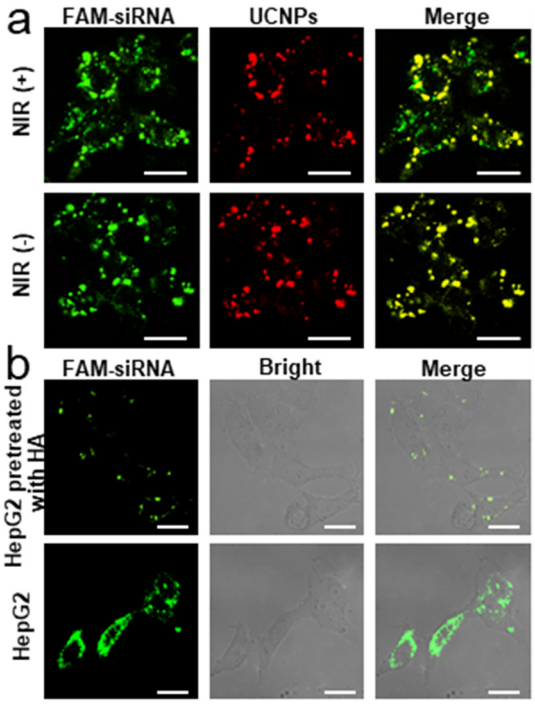

Figure 4. Confocal microscopic images of (**a**) co-localization of UCNPs at 454 nm and 475 emission and FAM-siRNA at 529 nm for PC-UCNPs/siRNA/HA-incubated HepG2 cells in the presence and absence of NIR irradiation (Scale bar: 25 μm), (**b**) PC-UCNPs/siRNA/HA-incubated HepG2 cells and PC-UCNPs/siRNA/HA-incubated HepG2 cells that pretreated free HA (Scale bar: 10 μm).

2.4. In Vitro Therapeutic Effect of PC-UCNPs/siRNA/HA

The polo-like family of serine/threonine protein kinases (PLKs) is the key to cell cycle regulation and proliferation, and PLK1 can promote oncogenic transformation; however, inhibiting PLK1 expression can cause mitotic catastrophe, cell cycle arrest and apoptosis [37,38]. Therefore, PLK1 siRNA was chosen as the sample siRNA and loaded to

PC-UCNPs to verify the therapeutic effect of PC-UCNPs/siRNA/HA. HepG2 cells were incubated with PC-UCNPs/siPLK1/HA for 6 h, irradiated with 980 nm light for 2 h (6 min intervals for every 10 min of light exposure to avoid heating), and continuously cultured for 24 h, and PLK1 mRNA expression and PLK1 protein expression were measured via qRT-PCR and enzyme-linked immunosorbent assay (ELISA), respectively. The PLK1 mRNA expression was down-regulated to 31% for the PC-UCNPs/siPLK1/HA-incubated HepG2 cells during NIR irradiation (Figure 5a, column 4), while PC-UCNPs/siPLK1/HA-incubated HepG2 cells showed 92% of mRNA expression in the absence of NIR irradiation (Figure 5a, column 2), and PC-UCNPs/siRNA'(nontherapeutic siRNA)/HA-incubated HepG2 cells showed 89% of mRNA expression during NIR irradiation (Figure 5a, column 3). The PLK1 protein expression in HepG2 cells with different treatments showed similar tendency with 36% of PLK1 protein expression for PC-UCNPs/siPLK1/HA-treated HepG2 cells during NIR irradiation (Figure 5b, column 4) and very limited suppressions of PLK1 protein expression for both PC-UCNPs/siPLK1/HA-treated HepG2 cells without NIR light irradiation (Figure 5b, column 2) and PC-UCNPs/siRNA' (nontherapeutic siRNA)/HA-treated HepG2 cells with NIR light irradiation (Figure 5b, column 3). In addition, PC-UCNPs/siPLK1/HA-treated Hela cells during NIR irradiation showed similar tendencies in mRNA expressions and PLK1 protein expressions (Figure S11a,b). These results demonstrated the satisfactory gene silencing efficiency and protein expression suppression of PC-UCNPs/siRNA/HA.

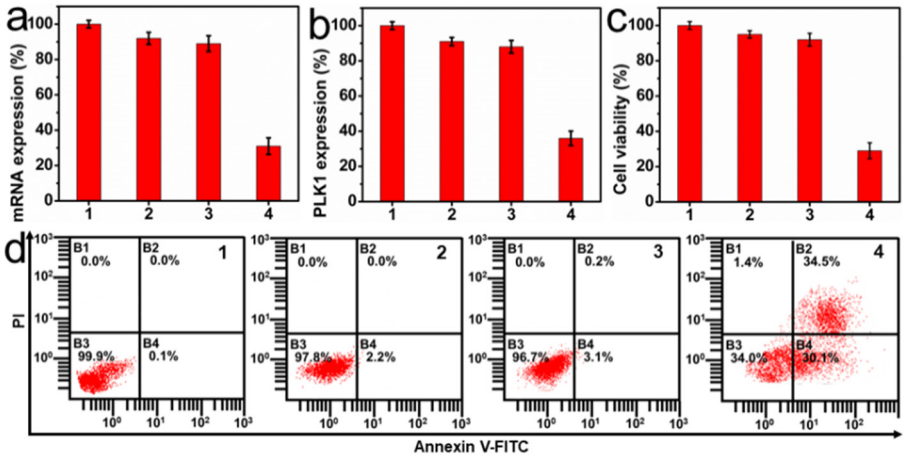

Figure 5. Gene silencing and cell viability. Expression levels of (**a**) PLK1 mRNA expression via qRT-PCR and (**b**) PLK1 protein expression via ELISA. Relative HepG2 cell viability determined via (**c**) MTT and (**d**) Annexin V-fluorescein isothiocyanate (FITC)/propidium iodide (PI) apoptotic kit. (1) Untreated HepG2 cells, (2) PC-UCNPs/siPLK1/HA-treated HepG2 cells without NIR irradiation, (3) PC-UCNPs/siRNA'/HA treated HepG2 cells with NIR irradiation and (4) PC-UCNPs/siPLK1/HA treated HepG2 cells with NIR irradiation. The error bars indicate means ± SD (n = 5).

The therapeutic effect of PC-UCNPs/siRNA/HA was evaluated using a standard MTT assay. HepG2 cells treated with PC-UCNPs/siPLK1/HA showed 29% of cell viability under NIR irradiation (Figure 5c, column 4), while cell viability was 96% for PC-UCNPs/siPLK1/HA-treated HepG2 cells in the absence of NIR irradiation (Figure 5c, column 2) and 94% for PC-UCNPs/siRNA'/HA-treated HepG2 cells under NIR irradiation (Figure 5c, column 3). Meanwhile, PC-UCNPs/siPLK1/HA-treated Hela cells showed 49% cell viability during NIR irradiation (Figure S11c). These results indicated the high therapeutic efficiency of PC-UCNPs/siRNA/HA. Flow cytometric assay results also showed the highest apoptosis rate of 64.6% for PC-UCNPs/siRNA/HA-treated HepG2 cells under NIR irradiation (Figure 5d). In addition, PC-UCNPs/siRNA/HA demonstrated satisfactory biocompatibility, with an 87% cell viability even at high concentrations, e.g., 200 μg/mL (Figure S11). Moreover, UCNPs/siRNA/HA showed a hemolysis percentage of 3.6% at a concentration of 1000 μg/mL (Figure S12), further indicating good biocompatibility.

2.5. In Vivo Therapeutic Efficiency of PC-UCNPs/siRNA/HA

Considering the overexpression of the CD44 receptor on the surface of the membrane, HepG2 cell tumor-bearing nude mice could be optimal tumor models [34]. The in vivo antitumor efficiency of PC-UCNPs/siPLK1/HA was evaluated using HepG2 cell tumor-bearing nude mice. PC-UCNPs/siPLK1/HA-injected mice after 2 h of NIR irradiation (6 min intervals for every 10 min of light exposure to avoid heating) showed the most effective inhibition of tumor growth compared with the PBS-treated mice group, and the PC-UCNPs/siPLK1/HA-treated mice group without NIR irradiation (Figure 6a), indicating the prominent in vivo antitumor capability of PC-UCNPs/siPLK1/HA. There was no noticeable body weight change in the mice during the treatment period (Figure 6b), indicating satisfactory biocompatibility and therapeutic specificity of PC-UCNPs/siPLK1/HA. All mice were euthanized on day 14, and the tumors were collected, weighed, sliced and stained using H&E and TUNEL to observe apoptosis via a CLSM image. PC-UCNPs/siPLK1/HA-treated mice group with NIR light irradiation also had the smallest tumor weight and size (Figure 6c,d) with the maximum disappearance of tumor nucleus in H&E images and the highest level of cell apoptosis in TUNEL images (Figure 6e). The in vivo applicability of PC-UCNPs/siRNA/HA was only evaluated for HepG2 cell tumor bearing mice and demonstrated satisfactory therapeutic efficiency. By conjugating with tumor targeting molecules, such as folic acid and aptamer AS1411, the as-presented PC-UCNPs/siRNA/HA nanoparticles could be widely suitable for a variety of tumor models.

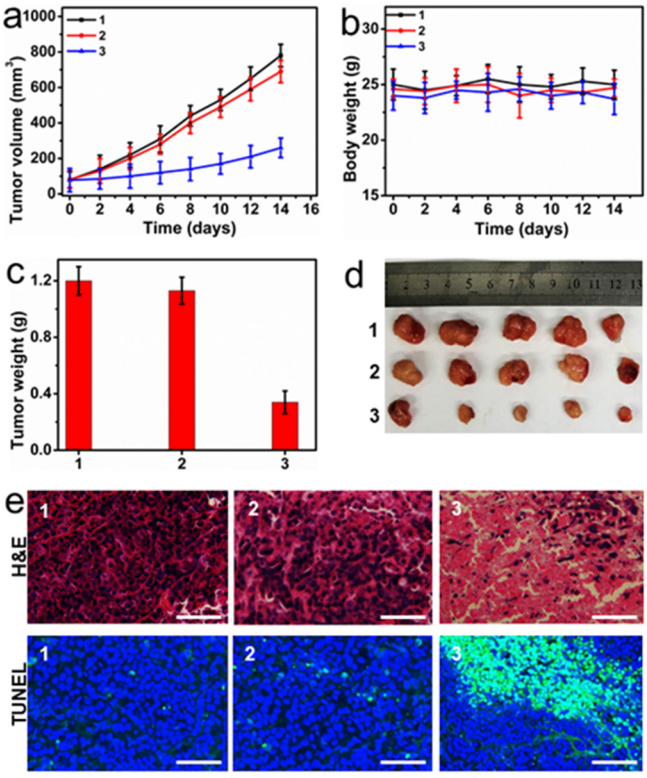

Figure 6. Demonstration of therapeutic efficiency with change of (**a**) tumor volume, (**b**) body weight of mice as a function of time, (**c**) tumor weight, (**d**) representative photos, (**e**) H&E staining and TUNEL staining of collected tumors for mice groups treated with PBS (1), PC-UCNPs/siPLK1/HA without NIR irradiation (2), PC-UCNPs/siPLK1/HA with NIR irradiation (3). The error bars indicate means ± SD (n = 5) (Scale bar, 100 μm).

3. Experimental

3.1. Materials and Reagents

Acryloyl chloride, 5-Hydroxy-2-nitrobenzaldehyde (98%), 2-(Dimethylamino) ethyl chloride hydrochloride (87%), Carbon disulfide (CS_2), 1-Propanethiol, 2-Bromo-2-methylpropionic acid, 1-

Ethyl-(3-dimethyllaminopropyl) carbodiie hydrochlide (EDC·HCl), N-Hydroxysuccinimide (NHS), (3-aminopropyl) triethoxysilane (APTES), Poly(oligo(ethylene glycol)) methyl ether acrylate (OEMA, Mn = 550 g/mol), 2,2′-Azoisobutyronitrile (AIBN) were purchased from J&K Chemical Co., Ltd. (Beijing, China). Anhydrous yttrium chloride (YCl_3) (99.9%), anhydrous ytterbium chloride ($YbCl_3$) (99.9%) and anhydrous thulium chloride ($TmCl_3$) (99.9%) were purchased from Sigma-Aldrich (Burlington, MA, USA). Tetraethylorthosilicate (TEOS), Sodium hydroxide (NaOH), Potassium phosphate (K_3PO_4), Ammonium fluoride (NH_4F), Cyclohexene, Oleic acid (OA), 1-Octadecene (ODE), Triethylamine (TEA), CO-520 surfactant, Tetraethyl orthosilicate (TEOS), (3-aminopropyl)triethoxysilane, Sodium borohydride ($NaBH_4$) were purchased from Alfa Aesar (Shanghai, China). Dulbecco's modified eagle's medium (DMEM), 4,6-Diamidino-2-phenylindole (DAPI), Trypsin, Penicillin streptomycin, 3-[4,5-dimethylthiazol-2-yl]-2,5-diphenyltetra-zoliumbromide (MTT), Fetal bovine serum (FBS), Phosphate buffered saline (PBS, pH 7.4), 6 x RNA loading buffer and Annexin V-FITC apoptosis detection kit were purchased from KeyGEN BioTECH (Nanjing, China). HepG2 human liver cancer cell lines were purchased from cell bank of Chinese Academy of Sciences. RNA extraction kit, PrimeScript RT reagent kit and SYBR premix EX Taq kit were purchased from Takara (Dalian, China). PLK1 ELISA kit was purchased from Jin Yibai Biological Technology (Shanghai, China). siRNA targeting PLK1 mRNA sequence (sense strand: 5′-AUAUUCGACUUUGGUUGCCTT-3′, antisense strand: 5′-GGCAACCAAAGUCGAAUAUTT-3′) and FAM fluorescein-labelled negative control siRNA sequence (FAM-siRNA) (sense strand: 5′-FAM-UUCUCCGAACGUGUCACGUTT-3′, antisense strand: 5′-ACGUGACACGUUCGGAGAATT-3′) were purchased from GenePharma Co., Ltd. (Shanghai, China). All other reagents and solvents were of analytical grade and used directly.

3.2. Apparatus

UV−Vis absorption spectra were recorded on a Nanodrop-2000C UV-Vis spectrophotometer (Nanodrop, Madison, WI, USA). Fourier-transform infrared (FT-IR) spectra were recorded on a Nicolet 6700 spectrophotometer (Nicolet Plastique, Nicolet, QC, Canada). Thermogravimetric analysis (TGA) was performed on a Setaram TGA 92 instrument (Setaram, Caluire-et-Cuire, France). Upconversion emission spectra were measured with a ZolixScan ZLX-UPL spectrometer (Beijing, China) with an external continuous-wave laser (980 nm) as the excitation source. Transmission electron microscopy (TEM) micrographs were acquired with JEM-2100 transmission electron microscope (JEOL Ltd., Tokyo, Japan), and confocal fluorescence images were acquired on TCS SP5 confocal laser scanning microscope (Leica, Frankfurt, Germany). Flow cytometric analysis was performed on a Coulter FC-500 flow cytometer (Beckman-Coulter, Pasadena, CA, USA). MTT and ELISA assays were performed on a Hitachi/Roche System Cobas 6000 (Bio-Rad, Hercules, CA, USA). Real-time PCR was carried out using a CFX96 touch real-time PCR detection system (Bio-Rad, Hercules, CA, USA). Zeta potential and dynamic light scattering (DLS) were measured via a Zetasizer Nano-ZS (Malvern Instruments, Malvern, UK) and ZetaPlus 90 Plus/BI-MAS (Brook Hhaven, New York, NY, USA), respectively.

3.3. Synthesis of 2-(((propanethio) carbonothioyl)thio)acetic Acid (CTA)

The 1-Propanethiol (548 mg, 7.19 mmol) was added to 10 mL acetone containing K_3PO_4 (1.53 g, 7.19 mmol) with magnetic stirring. After stirring for 10 min, CS_2 (1.64 g, 21.56 mmol) was added, and the reaction continued for 10 min. Additionally, 2-bromo-2-methylpropionic acid (1 g, 5.99 mmol) was then added and stirred overnight. The solvent was removed, and the residue was extracted using CH_2Cl_2 and 1 M HCl aqueous solution. The collected organic phase was then washed with water and dried using anhydrous Na_2SO_4, and the CH_2Cl_2 was removed via rotary evaporation. The crude product was further purified via recrystallization with hexane to obtain a yellow product (3.07 g, 65% yield). Moreover, ^{1}H-NMR ($CDCl_3$, 400 MHz, 298 K) δ (ppm): 3.27 (t, 2H), 1.78–1.67 (m, 8H), 1.00 (t, 3H) (Figure S1).

3.4. Synthesis of 5-(2-(dimethylamino)ethoxy)-2-nitrobenzyl Acrylate (MENA) Monomer

Synthesis of 5-hydroxy-2-nitrobenzyl alcohol (Compound 1): 5-hydroxy-2-nitrobenzaldehyde (500 mg, 3 mmol) in 10 mL methanol was syringed into the Schleck flask in an ice water bath under N_2 protection, $NaBH_4$ (226 mg, 5 mmol) was then slowly added, and the solution was stirred at 0 °C for 24 h. The reaction was cautiously quenched by the addition of a 10% HCl solution, adjusted to a pH of 2, and extracted using ethyl acetate. Organic layer was collected, washed with saturated NaCl solution, dried with anhydrous $MgSO_4$, filtered, and concentrated by a rotary evaporator. The crude product was further purified via silica gel column chromatography (hexane/ethyl acetate, $v/v = 1/1$). In addition, 5-hydroxy-2-nitrobenzyl alcohol (Compound 1) was obtained as a yellowish solid (705 mg, 97% yield). ^{1}H NMR (DMSO-d_6, 400 MHz, 298 K) δ (ppm): 10.88 (s, 1H, Ar–OH), 8.04, 7.24 and 6.78 (m, 3H, Ar), 5.5 (s, 1H, –CH_2OH), 4.81 (s, 2H, –CH_2OH) (Figure S3).

Synthesis of 5-(2-(dimethylamino)ethoxy)-2-nitrobenzyl alcohol (Compound 2): the mixture of compound 1 (500 mg, 2.96 mmol), 2-(dimethylamino)ethyl chloride hydrochloride (381 mg, 3.05 mmol) and NaOH (260 mg, 6.5 mmol) were added into a Schleck flask with both 15 mL toluene and 3 mL ethanol under N_2 protection. The reaction mixture was refluxed at 120 °C for 48 h and poured into 30 mL water after cooling. The organic layer was isolated, washed with saturated NaCl solution, dried over anhydrous Na_2SO_4, and concentrated by rotary evaporator. The as-obtained crude product was further purified via silica gel column chromatography using methanol as the eluent, and 5-(2-(dimethylamino)ethoxy)-2-nitrobenzyl alcohol (Compound 2) was obtained as a yellowish solid (572 mg, 65% yield). ^{1}H NMR ($CDCl_3$, 400 MHz, 298 K) δ (ppm): 8.16, 7.26, and 6.93 (m, 3H, Ar), 5.00 (s, 2H, –CH_2OH), 4.24 (t, 2H, –$OCH_2CH_2N(CH_3)_2$), 2.86 (t, 2H, –$OCH_2CH_2N(CH_3)_2$), 2.43 (s, 6H, –$OCH_2CH_2N(CH_3)_2$) (Figure S4).

Synthesis of 5-(2-(dimethylamino)ethoxy)-2-nitrobenzyl acrylate (MENA): Compound 2 (500 mg, 2.08 mmol) was added to the mixture solution of 7 mL anhydrous THF and 333 µL TEA at 0 °C under N_2 protection. Acryloyl chloride (198 µL, 2.185 mmol) in 500 µL anhydrous THF was then added dropwise. After reaction for 5 h at room temperature, the insoluble salts were removed via filtration. The filtrate was concentrated and further purified using silica gel column chromatography (hexane/ethyl acetate, $v/v = 3/1$) as the eluent. Additionally, 5-(2-(dimethylamino)ethoxy)-2-nitrobenzyl acrylate (MENA) was obtained as a yellowish solid (380 mg, 73% yield). ^{1}H NMR ($CDCl_3$, 400 MHz, 298 K) δ (ppm): 8.22, 7.09, and 6.94 (m, 3H, Ar), 6.54 (d, 1H, $CHCOOCH_2$–), 6.26 (m, 1H, $CHCOOCH_2$–), 5.95 (d, 1H, $CHCOOCH_2$–), 5.64 (2, 2H, Ar-CH_2O-), 4.21 (t, 2H, –$OCH_2CH_2N(CH_3)_2$), 2.86 (t, 2H, –$OCH_2CH_2N(CH_3)_2$), 2.42 (s, 6H, –$OCH_2CH_2N(CH_3)_2$) (Figure S5).

3.5. Synthesis of Core-Shell UCNPs: $NaYF_4$:Yb,Tm@$NaYF_4$

The UCNPs core $NaYF_4$:Yb,Tm was synthesized according to the previous report [39]. Briefly, YCl_3 (0.78 mmol), $YbCl_3$ (0.2 mmol), and $TmCl_3$ (0.02 mmol) were mixed with 6 mL OA and 15 mL ODE, heated to 150 °C and stirred for 2 h to remove oxygen and water. After cooling down to 30 °C, NH_4F (4 mmol) and NaOH (2.5 mmol) in 10 mL methanol were added dropwise into the mixture solution within 15 min. The reaction solution was then heated to 45 °C for 30 min, 90 °C for 30 min and 310 °C for 1 h under N_2 protection. The reaction solution was then cooled to room temperature and precipitated with the mixture of ethanol and acetone to obtain UCNPs core and re-dispersed in cyclohexane for further use.

For the synthesis of core–shell structured UCNPs $NaYF_4$:Yb,Tm@$NaYF_4$, YCl_3 (0.08 mmol) were mixed in ODE (15 mL) and OA (6 mL), heated to 150 °C, stirred for 2 h and subsequently cooled down to 75 °C. The above-obtained UCNPs core $NaYF_4$:Yb,Tm was added into the reaction mixture, and the reaction mixture was heated to 90 °C to remove the cyclohexane. After cooling to room temperature, NH_4F (4 mmol) and NaOH (2.5 mmol) in 10 mL methanol were added and continuously stirred at 45 °C for 30 min, at 90 °C for 30 min and at 290 °C for 45 min under N_2 protection to obtain core–shell structured UCNPs

$NaYF_4$:Yb,Tm@$NaYF_4$. The as-obtained UCNPs $NaYF_4$:Yb,Tm@$NaYF_4$ were precipitated with ethanol and re-dispersed in 10 mL of cyclohexane for future use. The morphology of as-prepared UCNPs was characterized by TEM, and its properties were characterized via fluorescence spectrometer.

3.6. Preparation of UCNPs@SiO_2-CTA

The UCNPs@SiO_2-NH_2 was synthesized via the reversed-phase microemulsion method according to the previous report with a slight modification [40]. Briefly, 500 μL CO-520 surfactant was added into 1 mg/mL of above-obtained UCNPs in 20 mL cyclohexane and sonicated for 10 min. A total of 100 μL $NH_3 \cdot H_2O$ (wt 30%) was added into the above mixture solution and continuously sonicated for 10 min until it formed a transparent solution. Then, 36 μL TEOS was added into the mixture solution, reacted for 3 h and centrifuged. The as-obtained UCNPs@SiO_2 was redispersed in ethanol, 400 μL of (3-aminopropyl)triethoxysilane and 70 μL of $NH_3.H_2O$ were added and stirred at 80 °C for 8 h. The as-obtained UCNPs@SiO_2-NH_2 was centrifuged and redispersed in DMSO for further use.

The mixture of CTA (20 mg, 0.08 mmol), NHS (9.7 mg, 0.08 mmol) and EDC·HCl (16.9 mg, 0.088 mmol) was added into 10 mL DMSO. After reaction for 4 h, the above-obtained UCNPs@SiO_2-NH_2 was added into the reaction solution, continuously reacted for 24 h, and centrifuged to obtain UCNPs@SiO_2-CTA. The property of UCNPs@SiO_2-CTA was characterized using UV-Vis spectrum.

3.7. Preparation of Photo-Cleavable Polycations-Wrapped UCNPs (PC-UCNPs)

The above obtained UCNPs@SiO_2-CTA (1.2 g), poly(oligo(ethylene glycol)) methyl ether acrylate (OEMA, 4.56 g, 9.6 mmol), MENA (744 mg, 2.4 mmol) and AIBN (12 mg) were added to a glass ampoule with anhydrous 1,4-dioxane (19.2 mL). The ampoule was degassed through three freeze–thaw cycles, sealed under vacuum, maintained in an oil bath preheated to 70 °C and kept for polymerization reaction for 24 h. The polymerization reaction was quenched with liquid nitrogen, and the reaction mixture was centrifuged at 8000 rpm for 5 min and washed with methanol. To endow positive charge to the as-obtained UCNPs@SiO_2-polymer, it (0.30 g) was dispersed in CH_2Cl_2 (30 mL), slowly added to CH_3I (0.1 g, 2 mmol) via a dropping funnel, and kept in the dark for 24 h at room temperature. The as-obtained PC-UCNPs was collected after centrifugation, dispersed in 10 mL PBS and stored at 4 °C for further use. The obtained PC-UCNPs were characterized via TEM, DLS and TG.

The gel permeation chromatographic (GPC) analysis of polycations coating of P(OEMA-co-MENA) was performed by dispersing above-obtained PC-UCNPs (200 mg) in hydrofluoric acid (HF, 5 mL), stirring it for 6 h at 50 °C and centrifuging it at 8000 rpm for 5 min. The supernatant was then collected, dialyzed (molecular weight cut off, 3.5 kDa) and freeze-dried. The obtained powder (1 mg) was mixed with THF (1 mL, mass spectrum grade) and analyzed by GPC using THF as eluent and polystyrene as reference polymer.

3.8. Preparation of siRNA-Loaded and HA-Wrapped PC-UCNPs (PC-UCNPs/siRNA/HA)

siRNA was loaded into the above-obtained PC-UCNPs via electrostatic interaction. After mixing 2 μg of siRNA in RNase-free DEPC with 2 μL of 6 X siRNA loading buffer, PC-UCNPs were added to PBS with a series of mass ratio (PC-UCNPs/siRNA (*w*/*w*) of 0, 0.6/1, 0.8/1, 1/1, 1.2/1), incubated at room temperature for 30 min and applied for the agarose gel retardation assay. Hyaluronic acid (HA) was then wrapped to the as-obtained PC-UCNPs/siRNA via electrostatic interaction to obtain PC-UCNPs/siRNA/HA. HA (50 mM) in PBS buffer was added into the prepared PC-UCNPs/siRNA with a mass ratio of 1/1, incubated for 10 min at room temperature and centrifuged at 8000 rpm for 5 min to obtain PC-UCNPs/siRNA/HA. The surface modification process was then characterized using zeta potential.

3.9. In Vitro Verification of HA Degradation and siRNA Release

PC-UCNPs/siRNA/HA was incubated with 0.5 mg/mL of HAase solution (HEPES buffer, pH 6.5) at 37 °C, and the degradation of HA was characterized by DLS and zeta potential over prearranged time intervals. To obtain the release profile of siRNA, the as-treated solutions were exposed under 980 nm of irradiation (2 W/cm^{-2}) for different durations, and the as-obtained solutions were centrifuged at predetermined time intervals. The supernatant containing released siRNA was measured via UV-Vis spectroscopy.

3.10. Cell Culture

The human hepatocellular carcinoma cells (HepG2, cancer cell) were incubated with DMEM medium containing 10% FBS and 1% penicillin-streptomycin (10,000 U/mL) at 37 °C in a humidified atmosphere containing 5% CO_2.

3.11. Intracellular Delivery of PC-UCNPs/siRNA/HA

To confirm the intracellular delivery specificity, HepG2 cells (CD44 receptor overexpression) were firstly pretreated with 2 mg/mL free HA at 37 °C for 1 h and then incubated with FAM-siRNA-loaded PC-UCNPs (PC-UCNPs/siRNA-FAM/HA, 5 μg/mL with siRNA 10 nM) for 6 h to observe FAM fluorescence using CLSM. Moreover, the fluorescence of directly PC-UCNPs/siRNA-FAM/HA-incubated HepG2 was observed.

3.12. Lysosomal Membrane Permeabilization of HepG2 Cells

To prove the lysosomal membrane permeabilization of HepG2 cells, HepG2 cells were incubated with PBS, UCNPs@SiO-polymer (in the absence of cationic quaternary ammonium groups), PC-UCNPs/HA, PC-UCNPs/siRNA/HA (5 μg/mL with siRNA 10 nM), respectively, for 6 h. The as-treated cells were stained with acridine orange (AO) (100 μL, 5 μg/mL) for 30 min, washed with PBS twice, and AO fluorescence was taken via CLSM.

3.13. Lysosomal Escape of siRNA

To verify the lysosomal escape of siRNA, HepG2 cells were incubated with 5 μg/mL of PC-UCNPs/siRNA-FAM/HA (siRNA 10 nM) for 2 h and 6 h, respectively. The as-treated cells were washed with PBS, incubated with 75 nM LysoTracker Green for 30 min, and observed via CLSM.

3.14. MTT Assay

To perform MTT assay, HepG2 cells (4000 cells/well) were seeded in a 96-well plate and incubated overnight in 200 μL of DMEM containing 10% FBS and 1% penicillin-streptomycin, the incubation medium was then replaced with 200 μL of fresh DMEM containing serial concentrations (40, 80, 120, 160 and 200 μg/mL) of PC-UCNPs/siRNA/HA and continuously incubated for 24 h. A total of 20 μL MTT (5 mg/mL in PBS) was subsequently added per well and continuously incubated for 4 h. After removing cell culture medium, 80 μL of DMSO was added to dissolve the crystals precipitate. The optical density was measured at 490 nm with a Bio-Rad microplate reader. Moreover, PBS-treated HepG2 cells were set as control group. The relative cell viability (%) was calculated using $(A_{test}/A_{control}) \times 100\%$.

SiRNA' with scrambled sequence and no biotoxicity was loaded to PC-UCNPs, and the as-obtained PC-UCNPs/siRNA'/HA was used to investigate the biotoxicity of PC-UCNPs/siRNA'/HA (siRNA 5 nM). Therapeutic siPLK1 was loaded to PC-UCNPs, and the as-obtained PC-UCNPs/siPLK1/HA (siPLK1 5 nM) was used to evaluate the therapeutic effect of PC-UCNPs/siPLK1/HA. PC-UCNPs/siPLK1/HA-incubated HepG2 cells were irradiated with the 980 nm laser (2 W/cm^2) for 2 h (6 min intervals for every 10 min of light exposure to avoid heating) and continuously incubated for 24 h for MTT assay. At the same time, Hela cells were also used to evaluate the therapeutic effect of PC-UCNPs/siPLK1/HA.

3.15. Hemolysis Assay of PC-UCNPs/siRNA/HA

Blood samples from healthy mice were collected in a container filled with heparin and centrifuged at 3000 rpm for 6 min to obtain red blood cells (RBCs). After washing and diluting with saline, RBCs (200 μL) were mixed with PC-UCNPs/siRNA/HA (800 μL) in saline at different concentrations (200, 400, 600, 800 and 1000 μg/mL) and incubated at 37 °C. After incubation for 4 h, the mixture solution was centrifuged, and the supernatant absorbance at 570 nm (A_{sample}) was measured via UV−vis. Moreover, RBCs were mixed with saline and water as a negative control (A_{saline}) and a positive control (A_{water}), respectively. The hemolysis percentage was calculated via $(A_{sample} - A_{saline})/(A_{water} - A_{saline}) \times 100\%$.

3.16. Gene Silencing Assay

HepG2 cells were seeded into a 6-well plate at a density of 5×10^5 cells/well and cultured at 37 °C overnight. The old medium was displaced with fresh medium containing PC-UCNPs/siPLK1/HA at siPLK1 concentrations of 250 nM, incubated for 4 h and exposed under 980 nm laser (2 W/cm^2) for 2 h (6 min intervals for every 10 min of light exposure to avoid heating). The as-treated HepG2 cells were continuously cultured for 24 h, and the expression levels of PLK1 mRNA and protein were evaluated using RT-PCR and ELISA kit following the manufacturer's instructions. The control group was set as siRNA' (scrambled sequence)-loaded PC-UCNPs/siRNA'/HA-treated HepG2 cells with NIR irradiation and PC-UCNPs/siPLK1/HA-treated HepG2 cells without NIR irradiation for the comparison of gene-silencing effect. Moreover, Hela cells were also adopted to evaluate the gene-silencing effect of PC-UCNPs/siPLK1/HA.

3.17. Cell Apoptosis Assay

HepG2 cells were seeded into a 6-well plate at a density of 2×10^5 cells/well and incubated with PC-UCNPs/siPLK1/HA at siPLK1 concentrations of 250 nM at 37 °C for 4 h, irradiated upon with a 980 nm laser for 2 h and continuously incubated for 24 h. Then, the as-treated cells were washed with PBS, stained with a mixture of 5.0 μL Annexin V-FITC and 5.0 μL propidium iodide for 10 min and measured with flow cytometry over FL1 (Annexin V-FITC) and FL3 (PI) channels. Control groups were set as siRNA' (scrambled sequence)-loaded PC-UCNPs/siRNA'/HA-treated HepG2 cells with NIR irradiation and PC-UCNPs/siPLK1/HA-treated HepG2 cells without NIR irradiation.

3.18. In Vivo Antitumor Efficiency

Pathogen-free female BALB/c nude mice were purchased from KeyGEN BioTECH (Nanjing, China). All experiment procedures were approved by the Model Animal Research Center of KeyGEN BioTECH. To build the tumor model in mice, HepG2 cells were only selected as models since their overexpressed CD44 receptor on the surface of membrane.1.0×10^7 HepG2 cells were subcutaneously injected to establish HepG2 tumor xenograft mouse model. After the tumor volumes grew to 50 mm^3, the tumor-bearing mice were randomly divided into three groups, with five mice in each group, and intratumorally injected, respectively, with 50 μL of PBS (1 group), PC-UCNPs/siPLK1/HA (2 groups) at a dose of 1 mmol siPLK1 per mouse. At 2 h post-injection, one of the PC-UCNPs/siPLK1/HA-injected mouse group was exposed to a 980 nm laser irradiation (2 W/cm^2) for 2 h (6 min intervals for every 10 min of light exposure to avoid heating). The injection and irradiation processes were repeated every other two days, a total of six times. The tumor sizes were measured every 2 days with caliper. The tumor volumes were calculated as $V = (L \times W^2)/2$, where L and W are the length and width of the tumor, respectively. To evaluate the safety of PC-UCNPs/siPLK1/HA in mice, the mice weights were also recorded during the therapeutic process. After treatment for 14 days, all mice were sacrificed, and the obtained tumors were then collected, weighed, photographed and stained using H&E and TUNEL.

4. Conclusions

Photo-cleavable polycations wrapping upconversion nanoparticles for the spatial and temporal control of siRNA delivery and release were presented. Photo-cleavable 5-(2-(dimethylamino)ethoxy)-2-nitrobenzyl acrylate and Poly(oligo(ethylene glycol)) methyl ether acrylate were polymerized in situ on the chain transfer agent CTA functionalized UCNPs@SiO_2 surface via RAFT polymerization, which was loaded with therapeutic PLK1 siRNA and HA for NIR-controlled in vivo siRNA release and tumor therapy. The as-presented PC-UCNPs/siPLK1/HA showed good inhibition of cell viability and tumor growth and should become a promising platform for precise drug delivery and tumor therapy.

Supplementary Materials: The following supporting information can be downloaded at: https://www.mdpi.com/article/10.3390/targets1010006/s1, Figure S1: Synthetic route and ^{1}H NMR spectrum (in $CDCl_3$) of chain transfer agent CTA; Figure S2: UV-Vis spectra of UCNPs@SiO_2, UCNPs@SiO_2-CTA and CTA; Figure S3: Synthetic route and ^{1}H NMR spectrum (in DMSO-d_6) of 5-hydroxy-2-nitrobenzyl alcohol (Compound 1).; Figure S4: Synthetic route and ^{1}H NMR spectrum (in $CDCl_3$) of 5-(2-(dimethylamino)ethoxy)-2-nitrobenzyl alcohol (Compound 2); Figure S5: Synthetic route and ^{1}H NMR spectrum (in $CDCl_3$) of 5-(2-(dimethylamino)ethoxy)-2-nitrobenzyl acrylate (DMNA); Figure S6: Synthetic route of UCNPs@SiO_2-polymer via RAFT polymerization; Figure S7: Gel permeation chromatographic (GPC) analysis of P(OEOA-co-DMNA) from the surface of UCNP@SiO_2-polymer using THF as eluent; Figure S8: Zeta potential and DLS analysis of UCNPs@SiO_2-polymer and PC-UCNPs; Figure S9: DLS analysis and polydispersity index (PDI) of PC-UCNPs/siRNA/HA incubated with DMEM containing 10% fetal bovine serum for different times; Figure S10: Semiquantitative analysis of intracellular FAM fluorescence intensity for PC-UCNPs/siRNA/HA incubated HepG2 cells and HA pre-treated HepG2 cells; Figure S11: Gene silencing and cell viability. Expression levels of (a) PLK1 mRNA expression via qRT-PCR, (b) PLK1 protein expression via ELISA and (c) relative Hela cell viability via MTT. (1) Untreated Hela cells, (2) PC-UCNPs/siPLK1/HA treated Hela cells without NIR irradiation, (3) PC-UCNPs/siRNA'/HA treated Hela cells with NIR irradiation, (4) PC-UCNPs/siPLK1/HA treated Hela cells with NIR irradiation. The error bars indicate means ± SD (n = 5).; Figure S12: Relative cell viabilities of HepG2 cells treated with PC-UCNPs/siRNA/HA at the series concentrations; Figure S13: Hemolysis percentages of red blood cells (RBCs) incubated with 0, 200, 400, 600, 800, 1000 μg/mL PC-UCNPs/siRNA/HA. The data error bars indicate means ± SD (n = 4).

Author Contributions: Y.H., S.G. and Y.L. are responsible for executing the methodology. Y.H. and S.G. handle the software and validation. The formal analysis, investigation, data curation, and writing of the original draft are carried out by Y.H., Y.L. and H.J. are responsible for the writing, review, editing, and acquisition of funding. All authors have read and agreed to the published version of the manuscript.

Funding: We gratefully acknowledge the National Natural Science Foundation of China (21974064, 22022405, 22101310, 82302278) and the State Key Laboratory of Analytical Chemistry for Life Science (5431ZZXM2204, 5431ZZXM2307).

Institutional Review Board Statement: The study was conducted in accordance with the Declaration of Animal Use and Care Regulations.

Informed Consent Statement: The study is not the involving human.

Data Availability Statement: The raw/processed data reported in this work are available upon request.

Conflicts of Interest: The authors declare no conflict of interest.

References

1. Conde, J.; Ambrosone, A.; Hernandez, Y.; Tian, F.; McCully, M.; Berry, C.C.; Baptista, P.V.; Tortiglione, C.; de la Fuente, J.M. 15 years on siRNA delivery: Beyond the state-of-the-art on inorganic nanoparticles for RNAi therapeutics. *Nano Today* **2015**, *10*, 421–450. [CrossRef]
2. Ozcan, G.; Ozpolat, B.; Coleman, R.L.; Sood, A.K.; Lopez-Berestein, G. Preclinical and clinical development of siRNA-based therapeutics. *Adv. Drug Deliv. Rev.* **2015**, *87*, 108–119. [CrossRef] [PubMed]

3. Kanasty, R.; Dorkin, J.R.; Vegas, A.; Anderson, D. Delivery materials for siRNA therapeutics. *Nat. Mater.* **2013**, *12*, 967–977. [CrossRef]
4. Liu, X.; Appelhans, D.; Voit, B.J. Hollow capsules with multiresponsive valves for controlled enzymatic reactions. *Am. Chem. Soc.* **2018**, *140*, 16106–16114. [CrossRef]
5. Wang, C.; Wang, X.; Du, L.; Dong, Y.; Hu, B.; Zhou, J.; Shi, Y.; Bai, S.; Huang, Y.; Cao, H.; et al. Harnessing pH-sensitive polycation vehicles for the efficient siRNA delivery. *ACS Appl. Mater. Interfaces* **2021**, *13*, 2218–2229. [CrossRef] [PubMed]
6. Li, R.; Huang, X.; Lu, G.; Feng, C. Characterization of a library of vitamin A-functionalized polymethacrylate-based nanoparticles for siRNA delivery. *Polym. Chem.* **2021**, *12*, 911–925.
7. Rapp, T.L.; DeForest, C.A. Targeting drug delivery with light: A highly focused approach. *Adv. Drug Deliv. Rev.* **2021**, *171*, 94–107. [CrossRef]
8. Lin, J.; Hu, J.; Wang, W.; Liu, K.; Zhou, C.; Liu, Z.; Kong, S.; Lin, S.; Deng, Y.; Guo, Z. Thermo and light-responsive strategies of smart titanium-containing composite material surface for enhancing bacterially anti-adhesive property. *Chem. Eng. J.* **2021**, *407*, 125783. [CrossRef]
9. Yang, X.; Chen, X.; Wang, Y.; Xu, G.; Yu, L.; Ding, J. Sustained release of lipophilic gemcitabine from an injectable polymeric hydrogel for synergistically enhancing tumor chemoradiotherapy. *Chem. Eng. J.* **2020**, *396*, 125320. [CrossRef]
10. Moroz-Omori, E.V.; Satyapertiwi, D.; Ramel, M.-C.; Høgset, H.; Sunyovszki, I.K.; Liu, Z.; Wojciechowski, J.P.; Zhang, Y.; Grigsby, C.L.; Brito, L.; et al. Photoswitchable gRNAs for spatiotemporally controlled CRISPR-Cas-based genomic regulation. *ACS Cent. Sci.* **2020**, *6*, 695–703. [CrossRef]
11. Li, S.; Xia, B.; Javed, B.; Hasley, W.D.; Melendez-Davila, A.; Liu, M.; Kerzner, M.; Agarwal, S.; Xiao, Q.; Torre, P.; et al. Direct visualization of vesicle disassembly and reassembly using photocleavable dendrimers elucidates cargo release mechanisms. *ACS Nano* **2020**, *14*, 7398–7411. [CrossRef]
12. Yang, S.; Pieters, P.A.; Joesaar, A.; Bögels, B.W.A.; Brouwers, R.; Myrgorodska, I.; Mann, S.; de Greef, T.F.A. Light-activated signaling in DNA-encoded sender–receiver architectures. *ACS Nano* **2020**, *14*, 15992–16002. [CrossRef] [PubMed]
13. Wang, S.-B.; Zhang, C.; Ye, J.-J.; Zou, M.-Z.; Liu, C.-J.; Zhang, X.-Z. Near-infrared light responsive nanoreactor for simultaneous tumor photothermal therapy and carbon monoxide-mediated anti-inflammation. *ACS Cent. Sci.* **2020**, *6*, 555–565. [CrossRef] [PubMed]
14. Li, Y.; Feng, P.; Wang, C.; Miao, W.; Huang, H. Black phosphorus nanophototherapeutics with enhanced stability and safety for breast cancer treatment. *Chem. Eng. J.* **2020**, *400*, 125851. [CrossRef]
15. Li, X.; Hu, H.; Shi, Y.; Liu, Y.; Zhou, M.; Huang, Z.; Li, J.; Ke, G.; Chen, M.; Zhang, X.-B. PtSnBi Nanoplates Enable Photoacoustic Imaging-Guided Highly Efficient Photothermal Tumor Ablation. *Chem. A Eng. J.* **2023**, *29*, e202203227. [CrossRef]
16. Wang, R.; Zhou, L.; Wang, W.; Li, X.; Zhang, F. In vivo gastrointestinal drug-release monitoring through second near-infrared window fluorescent bioimaging with orally delivered microcarriers. *Nat. Commun.* **2017**, *8*, 14702. [CrossRef] [PubMed]
17. Yang, Y.; Chen, Y.; Pei, P.; Fan, Y.; Wang, S.; Zhang, H.; Zhao, D.; Qian, B.-Z.; Zhang, B.-Z. Fluorescence-amplified nanocrystals in the second near-infrared window for in vivo real-time dynamic multiplexed imaging. *Nat. Nanotechnol.* **2023**, *6*, 1–10. [CrossRef]
18. Yan, B.; Boyer, J.C.; Branda, N.R.; Zhao, Y. Near-infrared light-triggered dissociation of block copolymer micelles using upconverting nanoparticles. *J. Am. Chem. Soc.* **2011**, *133*, 19714–19717. [CrossRef]
19. Wang, X.; Hu, J.; Liu, G.; Tian, J.; Wang, H.; Gong, M.; Liu, S. Reversibly switching bilayer permeability and release modules of photochromic polymersomes stabilized by cooperative noncovalent interactions. *J. Am. Chem. Soc.* **2015**, *137*, 15262–15275. [CrossRef]
20. Chen, G.; Ma, B.; Xie, R.; Wang, Y.; Dou, K.; Gong, S. NIR-induced spatiotemporally controlled gene silencing by upconversion nanoparticle-based siRNA nanocarrier. *J. Control. Release* **2018**, *282*, 148–155. [CrossRef]
21. Xie, S.; Du, Y.; Zhang, Y.; Wang, Z.; Zhang, D.; He, L.; Qiu, L.; Jiang, J.; Tan, W. Aptamer-based optical manipulation of protein subcellular localization in cells. *Nat. Commun.* **2020**, *11*, 1347. [CrossRef]
22. Wang, M.; Han, Y.; Yu, X.; Liang, L.; Chang, H.; Yeo, D.C.; Wiraja, C.; Wee, M.L.; Liu, L.; Liu, X.; et al. Upconversion Nanoparticle Powered Microneedle Patches for Transdermal Delivery of siRNA. *Adv. Healthcare Mater.* **2020**, *9*, 1900635. [CrossRef]
23. Zhang, Y.; Ren, K.; Zhang, X.; Chao, Z.; Yang, Y.; Ye, D.; Dai, Z.; Liu, Y.; Ju, H. Photo-tearable tape close-wrapped upconversion nanocapsules for near-infrared modulated efficient siRNA delivery and therapy. *Biomaterials* **2018**, *163*, 55–66. [CrossRef] [PubMed]
24. Wu, M.; Meng, Q.; Chen, Y.; Du, Y.; Zhang, L.; Li, Y.; Zhang, L.; Shi, J. Large-pore ultrasmall mesoporous organosilica nanoparticles: Micelle/precursor co-templating assembly and nuclear-targeted gene delivery. *Adv. Mater.* **2015**, *27*, 215–222. [CrossRef]
25. Lai, W.F.; Rogach, A.L.; Wong, W.T. Molecular design of upconversion nanoparticles for gene delivery. *Chem. Sci.* **2017**, *8*, 7339–7358. [CrossRef] [PubMed]
26. Kim, H.S.; Son, Y.J.; Mao, W.; Leong, K.W.; Yoo, H.S. Atom transfer radical polymerization of multishelled cationic corona for the systemic delivery of siRNA. *Nano Lett.* **2018**, *18*, 314–325. [CrossRef] [PubMed]
27. Martins, J.N.; Raimundo, B.; Rioboo, A.; Folgar-Cameán, Y.; Montenegro, J.; Basílio, N. Photoswitchable Calixarene Activators for Controlled Peptide Transport across Lipid Membranes. *J. Am. Chem. Soc.* **2023**, *145*, 13126–13133. [CrossRef] [PubMed]
28. Yonezawa, S.; Koide, H.; Asai, T. Recent advances in siRNA delivery mediated by lipid-based nanoparticles. *Adv. Drug Deliv. Rev.* **2020**, *154–155*, 64–78. [CrossRef]

29. Li, F.; Wang, M.; Guan, S.; Huang, Z.; Liu, S.; Li, X.; Jiang, X.; Luo, Q.; Xu, J.; Liu, J. Cucurbit[8]uril-based supramolecular polymer nanocapsules as an effective siRNA delivery platform for gene therapy. *Polym. Chem.* **2019**, *10*, 5659–5664. [CrossRef]
30. Haase, M.; Schafer, H. Upconverting nanoparticles. *Angew. Chem. Int. Ed.* **2011**, *50*, 5808–5829. [CrossRef]
31. Wang, Y.; Tu, L.; Zhao, J.; Sun, Y.; Kong, X.; Zhang, H. Upconversion Luminescence of β-NaYF4: Yb3+, Er3+@β-NaYF4 Core/Shell Nanoparticles: Excitation Power Density and Surface Dependence. *J. Phys. Chem. C* **2009**, *113*, 7164–7169. [CrossRef]
32. Xia, A.; Chen, M.; Gao, Y.; Wu, D.; Feng, W.; Li, F. Gd3+ complex-modified NaLuF4-based upconversion nanophosphors for trimodality imaging of NIR-to-NIR upconversion luminescence, X-Ray computed tomography and magnetic resonance. *Biomaterials* **2012**, *33*, 5394–5405. [CrossRef] [PubMed]
33. Malcolm, D.W.; Varghese, J.J.; Sorrells, J.E.; Ovitt, C.E.; Benoit, D.S.W. The Effects of Biological Fluids on Colloidal Stability and siRNA Delivery of a pH-Responsive Micellar Nanoparticle Delivery System. *ACS Nano* **2018**, *12*, 187–197. [CrossRef] [PubMed]
34. He, Y.; Guo, S.; Wu, L.; Chen, P.; Wang, L.; Liu, Y.; Ju, H. Near-infrared boosted ROS responsive siRNA delivery and cancer therapy with sequentially peeled upconversion nano-onions. *Biomaterials* **2019**, *225*, 119501. [CrossRef]
35. Gu, T.-T.; Li, C.; Xu, Y.; Zhang, L.; Shan, X.; Huang, X.; Guo, L.; Chen, K.; Wang, X.; Ge, H.; et al. Stimuli-responsive combination therapy of cisplatin and Nrf2 siRNA for improving antitumor treatment of osteosarcoma. *Nano Res.* **2020**, *13*, 630–637. [CrossRef]
36. Park, S.-J.; Park, W.; Na, K. Tumor Intracellular-Environment Responsive Materials Shielded Nano-Complexes for Highly Efficient Light-Triggered Gene Delivery without Cargo Gene Damage. *Adv. Funct. Mater.* **2015**, *25*, 3472–3482. [CrossRef]
37. Liu, F.; Park, J.-E.; Qian, W.-J.; Lim, D.; Gräber, M.; Berg, T.; Yaffe, M.B.; Lee, K.S.; Burke, T.R. Serendipitous alkylation of a Plk1 ligand uncovers a new binding channel. *Nat. Chem. Biol.* **2011**, *7*, 595–601. [CrossRef]
38. Barr, F.A.; Sillje, H.H.; Nigg, E.A. Polo-like kinases and the orchestration of cell division. *Nat. Rev. Mol. Cell Biol.* **2004**, *5*, 429–440. [CrossRef]
39. Liu, B.; Li, C.; Yang, P.; Hou, Z.; Lin, J. 808-nm-Light-excited lanthanide-doped nanoparticles: Rational design, luminescence control and theranostic applications. *Adv. Mater.* **2017**, *29*, 1605434. [CrossRef]
40. Sivakumar, S.; Diamente, P.R.; van Veggel, F.C. Silica-Coated Ln3+-Doped LaF3 Nanoparticles as Robust Down- and Upconverting Biolabels. *Chem. Eur. J.* **2006**, *12*, 5878–5884. [CrossRef]